Balanced Source Terms for Wave Generation Within Hasselmann Equation

Vladimir Zakharov[1,2,3,4], Donald Resio[5], and Andrei Pushkarev[1,2,3,4]

[1]Department of Mathematics, University of Arizona, Tucson, AZ 85721, USA
[2]Lebedev Physical Institute RAS, Leninsky 53, Moscow 119991, Russia
[3]Novosibirsk State University, Novosibirsk, 630090, Russia
[4]Waves and Solitons LLC, 1719 W. Marlette Ave., Phoenix, AZ 85015, USA
[5]Taylor Engineering Research Institute, University of North Florida

Correspondence to: Andrei Pushkarev (dr.push@gmail.com)

Abstract.

The new ZRP wind input source term (Zakharov et al., 2012) is examined for its theoretical consistency via numerical simulation of Hasselmann equation. The results are compared to field experimental data, collected at different sites around the world, and theoretical predictions based on self-similarity analysis. Consistent results are obtained for both limited fetch and duration limited statements.

1 Introduction

The scientific description of wind driven wave seas, inspired by solid state physics statistical ideas (see, for instance, Nordheim (1928)), was proposed by Hasselmann (1962, 1963) in the form of the kinetic equation for waves:

$$\frac{\partial \varepsilon}{\partial t} + \frac{\partial \omega_k}{\partial \boldsymbol{k}} \frac{\partial \varepsilon}{\partial \boldsymbol{r}} = S_{nl} + S_{in} + S_{diss} \tag{1}$$

where $\varepsilon = \varepsilon(\omega_k, \theta, \boldsymbol{r}, t)$ is the wave energy spectrum, as a function of wave dispersion $\omega_k = \omega(k)$, angle θ, two-dimensional real space coordinate $\boldsymbol{r} = (x, y)$ and time t. S_{nl}, S_{in} and S_{diss} are the nonlinear, wind input and wave-breaking dissipation source terms, respectively. Hereafter, only the deep water case, $\omega = \sqrt{gk}$ is considered, where g is the gravity acceleration and $k = |\boldsymbol{k}|$ is the absolute value of the vector wavenumber $\boldsymbol{k} = (k_x, k_y)$.

Since Hasselmann's work, Eq.(1) has become the basis of operational wave forecasting models such as WAM, SWAN and Wavewatch III (Tolman, 2013; SWAN). While the physical oceanography community consents on the general applicability of Eq.(1), there is no consensus agreement on universal parameterizations of the source terms S_{nl}, S_{in} and S_{diss}.

The S_{nl} term was derived by different methods from the Euler equations for free surface incompressible potential flow of a liquid by Hasselmann (1962, 1963) and Zakharov and Filonenko (1966). This term is a complex nonlinear operator acting on ε_k, concealing hidden symmetries (Zakharov and Filonenko, 1967; Zakharov et al., 1992). Resio and Perrie (1991) showed

that those different forms are identical on the resonant surface

$$\omega_{\boldsymbol{k_1}} + \omega_{\boldsymbol{k_2}} = \omega_{\boldsymbol{k_3}} + \omega_{\boldsymbol{k_4}} \quad (2)$$

$$\boldsymbol{k_1} + \boldsymbol{k_2} = \boldsymbol{k_3} + \boldsymbol{k_4} \quad (3)$$

The accuracy advantage of knowing the analytical expression for the S_{nl} term, known in physical oceanography as XNL, is overshadowed by its computational complexity. Today, none of the operational wave forecasting models can afford performing XNL computations in real time. Instead, the operational approximation, known as the DIA and its derivatives, are used to approximate this source term.. The implication of such simplification is the inclusion of a tuning coefficient in front of nonlinear term; however, several publications have now shown that the DIA does not provide a good approximation of the actual form of XNL. Consequently, other source terms must be adjusted to allow the model Eq.(1) to obtain desirable results.

In contrast to S_{nl}, the knowledge of the S_{in} and S_{diss} source terms is poor, and both now include many heuristic factors and coefficients.

The creation of a reliable, well justified theory of S_{in} has been hindered by strong turbulent fluctuations in boundary layer over the sea surface. Even one of the most crucial elements of this theory, the vertical distribution of horizontal wind velocity in the region closest to the ocean surface, where wave motions strongly interact with atmospheric motions, is still the subject of the debate. The history of the development of different wind input forms is full of assumptions, which fundamentally restrict the magnitude and directional distribution of this term. As a result, the values of different wind input terms scatter by a factor of $300 \div 500\%$ (Badulin et al., 2005; Pushkarev and Zakharov, 2016). Additional information on this detailed analysis of current state of wind input terms can be found in Pushkarev and Zakharov (2016).

Similar to the wind input term, there is little consent on the parameterization of the source dissipation term S_{diss}. The physical dissipation mechanism, which most physical oceanographers agree on, is the effect of wave energy loss due to wave breaking, while there are also other dubious ad-hoc "long wave" dissipation source terms, having heuristically justified physical explanations. Currently, there is not even an agreement on the localization of wave breaking events in Fourier space. The approach currently utilized in operational wave forecasting models mostly relies on the dissipation, localized in the vicinity of the spectral energy peak. Recent numerical experiments show (Pushkarev and Zakharov, 2016; Dyachenko et al., 2015; Zakharov et al., 2009), however, that such approach does not pass most of the tests associated with the essentially nonlinear nature of the Eq.(1).

Wave breaking dissipation, known also as "white-capping dissipation", is an important physical phenomenon, not properly studied yet for the reasons of mathematical and technological complexity. Longuet-Higgins (1980a, b) achieved important results, but didn't accomplish the theory completely. Irisov and Voronovich (2011) studied wave-breaking of the short waves, "squeezed" by surface currents, caused by longer waves, and showed that they become steep and unstable. Our explanation is simpler, but has the same consequences: the "wedge" formation, preceding the wave breaking, causes the "fat tail" appearance in Fourier space. Subsequent smoothing of the tip of the wedge is equivalent to the "chopping off" of the developed high-frequency tail – a sort of natural low-pass filtering – leading to the loss of the wave energy. This effect is referred as "cigar

cutting effect" (Pushkarev and Zakharov, 2016). Both scenarios have the same consequences of wave surface smoothing, and are indirectly confirmed by presented numerical experiments in that study.

Instead of following the previous path of time-consuming numerical and field experiments, the authors of the current manuscript are pursuing an alternative approach to defining the S_{in} and S_{diss} terms . Based on the leading nonlinearity role in Eq.(1) ((Zakharov, 2010; Zakharov and Badulin, 2011)), it was decided to analyze a multi-parametric family of self-similar solutions of Eq.(1). The comparison with the results of field observations allowed to find a new wind input form, herein termed the ZRP S_{in} wind input source term (Zakharov et al., 2012). The wave breaking dissipation term S_{diss} has been chosen in the form of "implicit dissipation" via Phillips $\sim f^{-5}$ spectral continuation tail. That framework reproduced the observations of a dozen of field experiments , i.e. self-similar exponents $p = 1$ and $q = -0.3$ of power dependencies of total wave energy $\sim \chi^p$ and spectral peak frequency $\sim \omega^q$ along a fetch (Pushkarev and Zakharov, 2016).

In the following section we are describing the details of ZRP model and pertaining numerical results in duration limited and fetch limited statements. The duration limited numerical simulation is the subject of more academic than applied interest with the purpose of self-simlarity concept support, while the limited fetch numerical simulation results, besides academic interest, are the subject of extensive comparison with the field experiments.

2 Experimental evidence

Here we examine the empirical evidence from around the world, which has been utilized to quantify energy levels within the equilibrium spectral range by Resio et al. (2004a). For convenience, we shall also use the same notation used by Resio et al. (2004a) in their study, for the angular averaged spectral energy densities in frequency and wavenumber spaces:

$$E_4(f) = \frac{2\pi\alpha_4 V g}{(2\pi f)^4} \tag{4}$$

$$F_4(k) = \beta k^{-5/2} \tag{5}$$

where $f = \frac{\omega}{2\pi}$, α_4 is the constant, V is some characteristic velocity and $\beta = \frac{1}{2}\alpha_4 V g^{-1/2}$. These notations are based on relation of spectral densities $E(f)$ and $F(k)$ in frequency $f = \frac{\omega}{2\pi}$ and wave-number k bases:

$$F(k) = \frac{c_g}{2\pi} E(f) \tag{6}$$

where $c_g = \frac{d\omega}{dk} = \frac{1}{2\cdot 2\pi}\frac{g}{f}$ is the group velocity.

The notations in Eqs.(4)-(5) are connected with the spectral energy density $\epsilon(\omega, \theta)$ through

$$E(f) = 2\pi \int \epsilon(\omega, \theta) d\theta \tag{7}$$

The Resio et al. (2004a) analysis showed that experimental energy spectra $F(k)$, estimated through averaging $< k^{5/2} F(k) >$, can be approximated by linear regression line as the function of $(u_\lambda^2 c_p)^{1/3} g^{-1/2}$. Fig.1 shows that the regression line

$$\beta = \frac{1}{2}\alpha_4 \left[(u_\lambda^2 c_p)^{1/3} - u_0 \right] g^{-1/2} \tag{8}$$

indeed, seems to be a reasonable approximation of these observations.

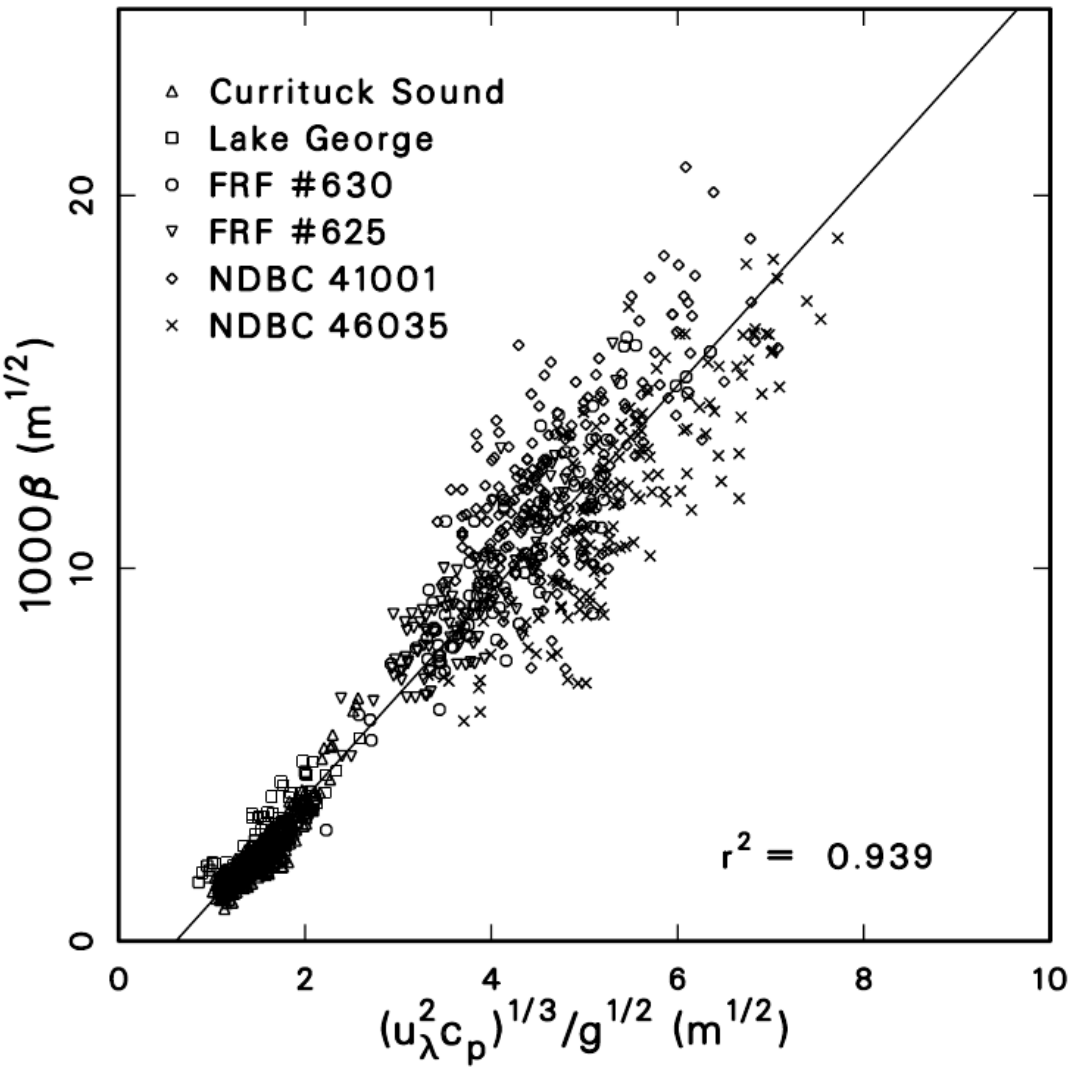

Figure 1. Correlation of equilibrium range coefficient β with $(u_\lambda^2 c_p)^{1/3}/g^{1/2}$ based on data from six disparate sources. Adapted from Resio et al. (2004a)

Here $\alpha_4 = 0.00553$, $u_0 = 1.93\ m/sec$, c_p is the spectral peak phase speed and u_λ is the wind speed at the elevation equal to a fixed fraction $\lambda = 0.065$ of the spectral peak wavelength $2\pi/k_p$, where k_p is the spectral peak wave number. It is important to emphasize that Resio et al. (2004a) experiments show that parameter β increases with development of the wind-driven sea, when f_p decreases and C_p increases. This observation is consistent with the weak turbulent theory, where $\beta \sim P^{1/3}$ (Zakharov et al., 1992); here P is the wave energy flux toward small scales.

Resio et al. (2004a) assumed that the near surface boundary layer can be treated as neutral and thus follows a conventional logarithmic profile

$$u_\lambda = \frac{u_\star}{\kappa} \ln \frac{z}{z_0} \tag{9}$$

having Von Karman coefficient $\kappa = 0.41$, where $z = \lambda \cdot 2\pi/k_p$ is the elevation equal to a fixed fraction $\lambda = 0.065$ of the spectral peak wavelength $2\pi/k_p$, where k_p is the spectral peak wave number, and $z_0 = \alpha_C u_\star^2/g$ subject to Charnock (1955) surface roughness with $\alpha_C = 0.015$.

3 Theoretical considerations

Self-similar solutions consistent with the conservative kinetic equation

$$\frac{\partial \epsilon(\omega,\theta)}{\partial t} = S_{nl} \tag{10}$$

were studied in Zakharov (2005), Badulin et al. (2005). In this section we study self-similar solutions of the forced kinetic equation

$$\frac{\partial \epsilon(\omega,\theta)}{\partial t} = S_{nl} + \gamma(\omega,\theta)\epsilon(\omega,\theta) \tag{11}$$

where $\epsilon(\omega,\theta) = \frac{2\omega^4}{g} N(\mathbf{k},\theta)$ is the energy spectrum.

One should note that this equation doesn't contain any explicit wave dissipation term, the role of dissipation is played by an infinite phase volume sink at high wave numbers, in spirit of the Weak Turbulent Theory (hearafter WTT), see Zakharov and Filonenko (1967), Zakharov et al. (1992).

For our purposes, it is sufficient to simply use the dimensional estimate for S_{nl},

$$S_{nl} \simeq \omega \left(\frac{\omega^5 \epsilon}{g^2}\right)^2 \epsilon \tag{12}$$

Eq.(11) has a self-similar solution if

$$\gamma(\omega,\theta) = \alpha \omega^{1+s} f(\theta) \tag{13}$$

where s is a constant. Looking for self-similar solution in the form

$$\epsilon(\omega,t) = t^{p+q} F(\omega t^q) \tag{14}$$

we find

$$q = \frac{1}{s+1} \tag{15}$$

$$p = \frac{9q-1}{2} = \frac{8-s}{2(s+1)} \tag{16}$$

The function $F(\xi)$ has the maximum at $\xi \sim \xi_p$, thus the frequency of the spectral peak is

$$\omega_p \simeq \xi_p t^{-q} \tag{17}$$

The phase velocity at the spectral peak is

$$c_p = \frac{g}{\omega_p} = \frac{g}{\xi_p} t^q = \frac{g}{\xi_p} t^{\frac{1}{s+1}} \tag{18}$$

According to experimental data, the main energy input into the spectrum occurs in the vicinity of the spectral peak, i.e. at $\omega \simeq \omega_p$. For $\omega >> \omega_p$, the spectrum is described by Zakharov-Filonenko tail

$$\epsilon(\omega) \sim P^{1/3} \omega^{-4} \tag{19}$$

Here

$$P = \int_0^\infty \int_0^{2\pi} \gamma(\omega,\theta)\epsilon(\omega,\theta) d\omega d\theta \tag{20}$$

This integral converges if $s < 2$. For large ω

$$\epsilon(\omega,t) \simeq \frac{t^{p-3q}}{\omega^4} \simeq \frac{t^{\frac{2-s}{2(s+1)}}}{\omega^4} \tag{21}$$

More accurately

$$\epsilon(\omega,t) \simeq \frac{\mu g}{\omega^4} u^{1-\eta} c_p^\eta g(\theta) \tag{22}$$

$$\eta = \frac{2-s}{2} \tag{23}$$

Now supposing $s = 4/3$ and $\gamma \simeq \omega^{7/3}$, we get $\eta = 1/3$, which is exactly experimental regression line prediction. Because it is known from regression line in Fig.1 that $\xi = 1/3$, we immediately get $s = 4/3$ and the wind input term

$$S_{wind} \simeq \omega^{7/3} \epsilon \tag{24}$$

At this step we are almost done with the construction of ZRP wind input term. The only missing component is an unknown coefficient in front of it, which will be defined later from the comparison with total energy growth in experimental observations.

Another important theoretical relationship, that can be derived from joint consideration of Eqs. (4), (6) and (22) is

$$1000\beta = \lambda \frac{(u^2 c_p)^{1/3}}{g^{1/2}} \tag{25}$$

which shows a theoretical equivalence to the experimental regression, where λ is an unknown constant, defined experimentally.

At the end of the section, we present the summary of important relationships.

Wave action N, energy E and momentum M in frequency-angle presentation are:

$$N = \frac{2}{g^2} \int_0^\infty \int_0^{2\pi} \omega^3 n d\omega d\phi \tag{26}$$

$$E = \frac{2}{g^2} \int_0^\infty \int_0^{2\pi} \omega^4 n d\omega d\phi \tag{27}$$

$$M = \frac{2}{g^3} \int_0^\infty \int_0^{2\pi} \omega^5 n \cos\phi d\omega d\phi \tag{28}$$

The self-similar relations for duration limited case are given by:

$$\epsilon = t^{p+q} F(\omega t^q) \tag{29}$$

$$9q - 2p = 1,\ p = 10/7,\ q = 3/7\ \ s = 4/3 \tag{30}$$

$$N \sim t^{p+q} \tag{31}$$

$$E \sim t^p \tag{32}$$

$$M \sim t^{p-q} \tag{33}$$

$$<\omega> \sim t^{-q} \tag{34}$$

The same sort of self-similar analysis gives self-similar relations for fetch limited case:

$$\epsilon = \chi^{p+q} F(\omega \chi^q) \tag{35}$$

$$10q - 2p = 1,\ p = 1,\ q = 3/10\ \ s = 4/3 \tag{36}$$

$$N \sim \chi^{p+q} \tag{37}$$

$$E \sim \chi^p \tag{38}$$

$$M \sim \chi^{p-q} \tag{39}$$

$$<\omega> \sim \chi^{-q} \tag{40}$$

3.1 The details of "implicit"dissipation

Now that the construction of ZRP wind input term with the unknown coefficient has been accomplished in spirit of WTT in the previous chapter, the HE model, suitable for numerical simulation still misses dissipation term, localized at finite wave numbers – there is no such thing as the inifinite phase volume in the reality: the real ocean Fourier space is confined by characteristic wave number, corresponding to the start of the dissipation effects, caused by the wave-breaking events.

There is a lot of freedom in choosing the dissipation term. Since there is no current interpretation of the wave-breaking dissipation mechanism, one can choose it in whatever shape it is preferred, but any particular choice will be questioned since it is an artificial one.

Because of that, the motivation consisted in the fact that at the current "proof if the concept" stage one need to know the effective sink with the simplest structure. Continuation of the spectrum from ω_{crit} with Phillips law $A(\omega_{crit}) \cdot \omega^{-5}$ (see Phillips (1966)), decaying faster than equlibrium spectrum ω^{-4}, will get high-frequency dissipation. The corresponding analytic parameterization of this dissipation term will be unknown, while not in principle impossible to figure out in some way. One should note that this method of dissipation is not our invention, it is described in Janssen (2009).

Specifically, the coefficient $A(\omega_{crit})$ in front of ω^{-5}, is unknown, but is not required to be defined in an explicit form. Instead, it is dynamically determined from the continuity condition of the spectrum, at frequency ω_{crit}, on every time step. In other

words, the starting point of the Phillips spectrum coincides with the last point of the dynamically changing spectrum, at the frequency point $\omega_{crit} = 2\pi f_{crit}$, where $f_{crit} \simeq 1.1\ Hz$, as per Long and Resio (2007). This is the way the high frequency "implicit" damping is incorporated into the alternative computational framework of HE. The question of the finer details of the high-frequency "implicit" damping structure is of secondary importance, at the current "proof of the concept" stage.

The whole set of the input and dissipation terms is accomplished now with one uncertainty: the explained approach leaves one parameter arbitrary – the constant in front of the wind input term. We choose it equal to 0.05 from the condition of the reproduction of the field observations of wave energy growth along the fetches, analyzed in Badulin et al. (2007).

4 Numerical validation of relationship

To check the self-similar hypothesis posed in Eq.(24), we performed a series of numerical simulations of Eq.(1) in the spatially homogeneous duration limited $\frac{\partial N}{\partial \boldsymbol{r}} = 0$ and spatially inhomogeneous fetch limited $\frac{\partial N}{\partial t} = 0$ situations.

All simulations used WRT (Webb-Resio-Tracy) method (see Tracy and Resio (1982)), which calculates the nonlinear interaction term in the exact form. The presented numerical simulation utilized the version of WRT method, previously used in Korotkevich et al. (2008); Resio and Perrie (1989); Perrie and Zakharov (1999); Resio et al. (2004b); Long and Resio (2007); Badulin and Zakharov (2012); Webb (1978), and used the grid of 71 logarithmically spaced points in the frequency range from $0.1Hz$ to $2.0Hz$ and 36 equidistant points in the angle domain. The constant time step in the range between 1 and 2 sec has been used for explicit first order accuracy order integration in time.

All numerical simulations discussed in the current paper have been started from uniform noise energy distribution in Fourier space, corresponding to small initial wave height with effectively negligible nonlinearity level. The constant wind of speed $10\ m/sec$ was assumed blowing away from the shore line, along the fetch. The assumption of the constant wind speed is a necessary simplification, due to the fact that the numerical simulation is being compared to various data from field experiments, and the considered set-up is the simplest physical situation, which can be modeled.

The same ZRP wind input term Eq.(24) has been used in both cases in the form

$$S_{in}(\omega,\phi) = \gamma(\omega,\phi)\cdot\varepsilon(\omega,\phi) \tag{41}$$

$$\gamma = 0.05\frac{\rho_{air}}{\rho_{water}}\omega\left(\frac{\omega}{\omega_0}\right)^{4/3} q(\theta) \tag{42}$$

$$\omega = 2\pi f, \quad f_{min} \le f \le f_d \tag{43}$$

$$q(\theta) = \begin{cases} \cos^2\theta \ \text{ for } -\pi/2 \le \theta \le \pi/2 \\ 0 \ \text{ otherwise} \end{cases} \tag{44}$$

$$\omega_0 = \frac{g}{U}, \ \frac{\rho_{air}}{\rho_{water}} = 1.3\cdot 10^{-3} \tag{45}$$

where U is the wind speed at the reference level of 10 meters, ρ_{air} and ρ_{water} are the air and water density correspondingly. It is conceivable to use more sophisticated expression for $q(\theta)$, for instance $q(\theta) = q(\theta) - q(0)$. To make direct comparison with experimental results of Resio et al. (2004a), we used the relation $u_\star \simeq U/28$ (see Golitsyn (2010)) in Eq.(9). The wind input function S_{in} was defined in the frequency domain 0.1 Hz $< f <$ 1.1 Hz.

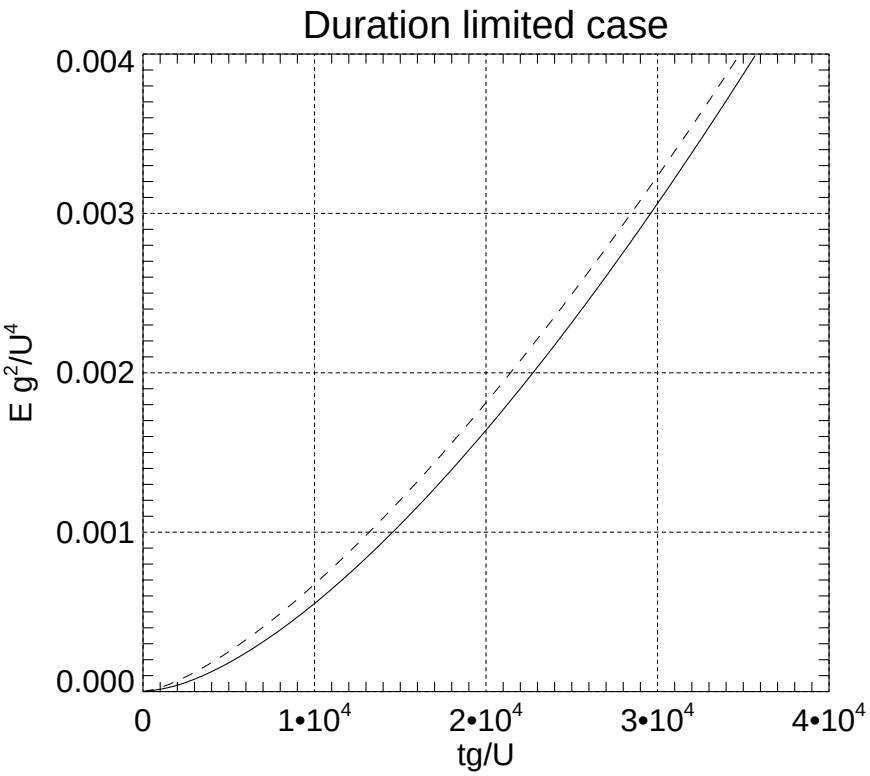

Figure 2. Dimensionless energy Eg^2/U^4 versus dimensionless time tg/U for wind speed $U = 10$ m/sec duration limited case - solid line. Self-similar solution with the empirical coefficient in front of it: $1.3 \cdot 10^{-9} \, (tg/U)^{10/7}$ - dashed line.

The above described "implicit dissipation" term S_{diss} has played dual role of direct energy cascade flux sink due to wave breaking as well as numerical scheme stabilization factor at high wavenumbers.

4.1 Duration limited numerical simulation

The duration limited simulation has been performed for a wind speed of $U = 10$ m/sec.

Fig.2 shows the total energy growth as the function of time, consistent with self-similar prediction Eq.(32) for index $p = 10/7$, supplied with the empirical coefficient in front of it, see Fig.3.

One should specifically elaborate on the local index p numerical calculation procedure for Fig.3. First, we smooth the total energy function via moving average, then calculate the corresponding derivative numerically through taking finite differences, and finally moving averaging the result. The parameters of moving averages have to be found individually in any specific case.

The relatively small systematic deviation from self-similar behavior, visible on Fig.2, is connected with two facts.

The first fact is the transition process in the beginning of the simulation, when the wave system behavior is far from self-similar one. But the self-similar solution is pure power function, without taking into account the initial transition process, and

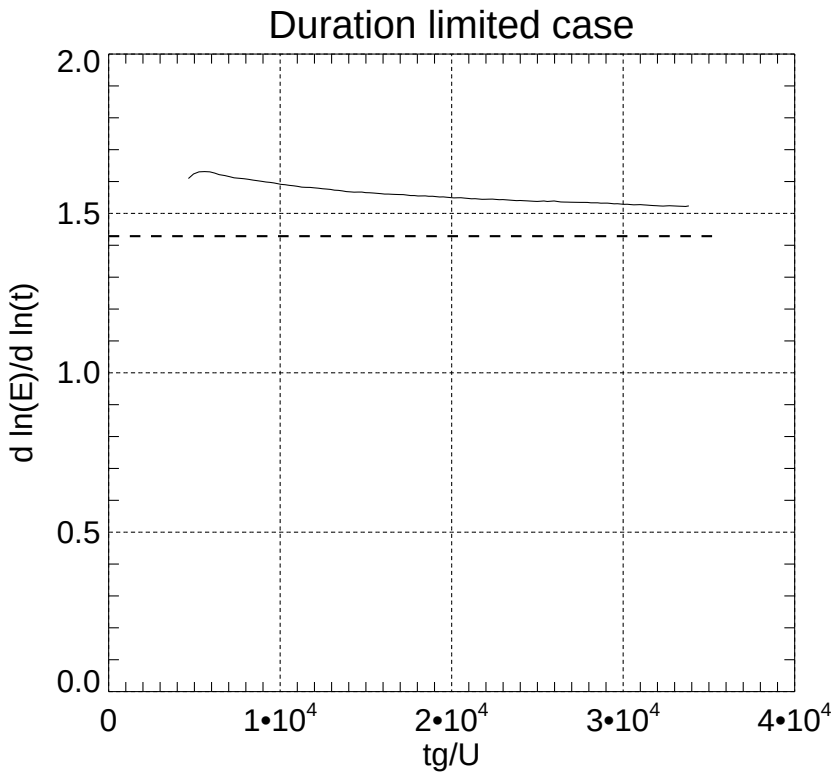

Figure 3. Energy local power function index $p = \frac{d\ln E}{d\ln t}$ as a function of dimensionless time tg/U for wind speed $U = 10$ m/sec duration limited case - solid line. Theorerical value of self-similar index $p = 10/7$ - thick horizontal dashed line.

that causes the systematic difference. This systematic difference could be diminished via a parallel shift, which would take into account the initial transition process. Such parallel shift is equivalent to starting the simulation from different initial conditions.

The second fact is the asymptotic nature of the self-similar solution, producing an evolution of the simulated wave system toward self-similar behavior with increasing time. As seen on Fig.3, the numerical value of the local exponent converges to the theoretical value $p = 10/7$, reaching approximately 6% accuracy for sufficient dimensionless time $3 \cdot 10^4$.

The dependence of the mean frequency on time, shown on Fig.4, is consistent with the self-similar dependence found in Eq.(34) for $q = 3/7$, supplied with the empirical coefficient in front of it, see Fig.5.

The systematic deviation of two lines on Fig.4, remain within 3% of the target value $q = 3/7$ for the same reasons as for wave energy behavior - the transition process in the beginning of the simulation and asymptotic nature of self-similar solution.

A check of the consistency with the "magic number" $9q - 2p = 1$ (see Eq.(30)), is presented on Fig.6. The reason of systematic deviation from the target value 1 is obviously connected with the reasons of the systematic deviations of p and q, as the "magic number" is calculated as their linear combination, reaching the accuracy of approximately 10% for a long enough dimensionless time of $3 \cdot 10^4$.

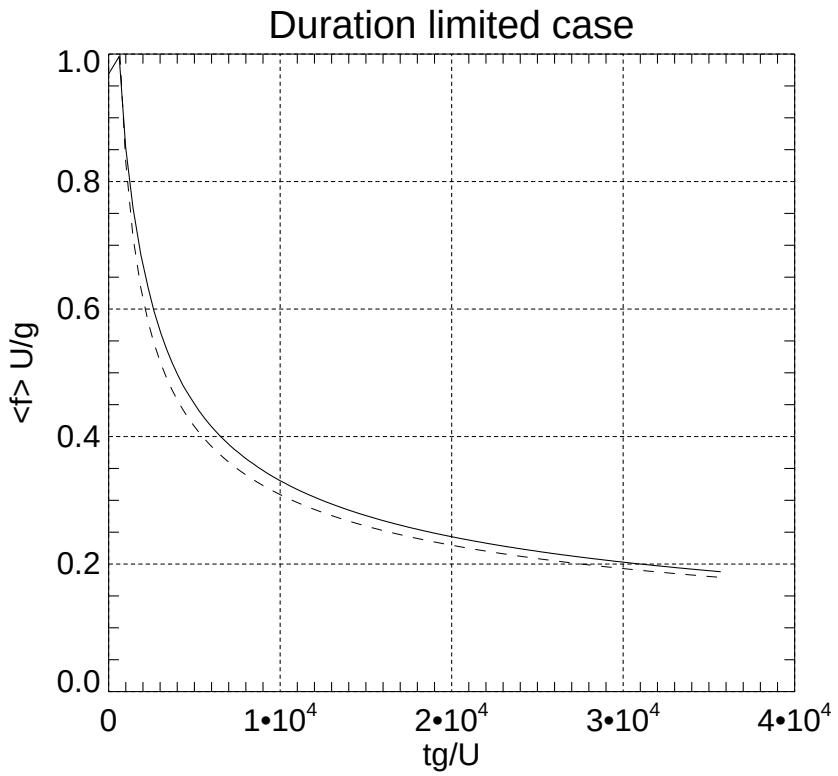

Figure 4. Dimensionless mean frequency $< f > \cdot U/g = E/N \cdot U/g$ (solid line) versus dimensionless time tg/U for wind speed $U = 10$ m/sec duration limited case - solid line, self-similar solution with the empirical coefficient in front of it: $16.0 \cdot (tg/U)^{-3/7}$ - dashed line.

One should not that indices p, q and the "magic relation" $9q - 2p$ exhibit asymptotic convergence to the corresponding target values.

Fig.7 presents angle-integrated energy spectrum, as the function of frequency, in logarithmic coordinates. One can see that it consists of the segments of:

- the spectral peak region
- the inertial (equilibrium) range ω^{-4} spanning from the spectral peak to the beginning of the "implicit dissipation" $f = 1.1$ Hz
- Phillips high frequency tail ω^{-5} starting approximately from $f = 1.1$ Hz

The compensated spectrum $F(k) \cdot k^{5/2}$ is presented in Fig.8.

One can see plateau-like region responsible for $k^{-5/2}$ behavior, equivalent to $\sim f^{-4}$ tail in Fig.7. This exact solution of Eq.(10), known as KZ spectrum, was found by Zakharov and Filonenko (1967). The universality of f^{-4} asymptotics for the "intertial" (also known as "equilibrium" in oceanography) range between spectral peak energy input and high-frequency

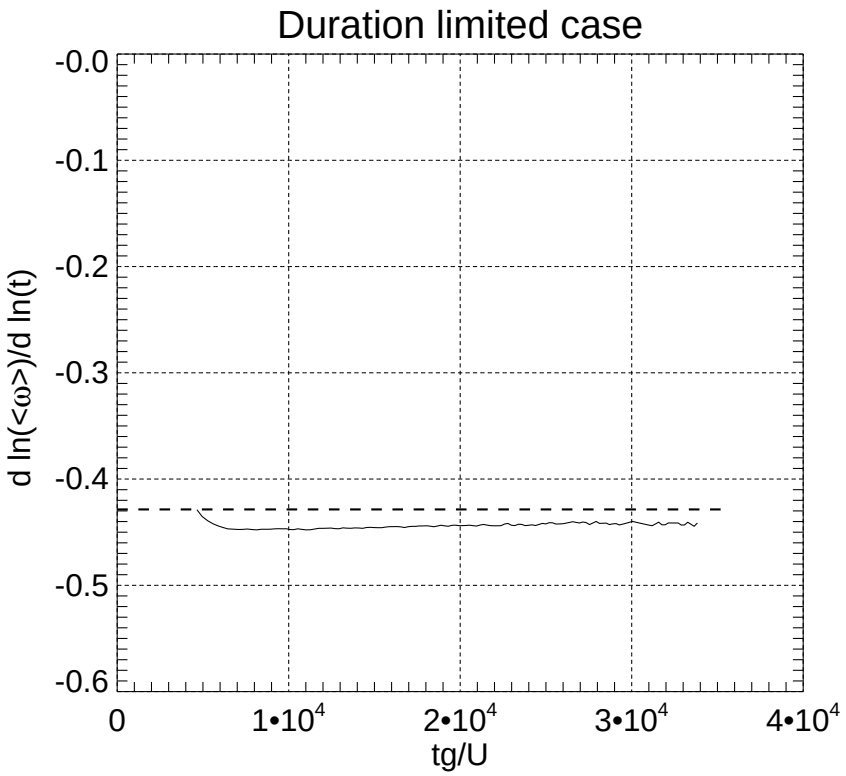

Figure 5. Mean frequency local power function index $-q = \frac{d\ln<\omega>}{d\ln t}$ as the function of dimensionless time tg/U for wind speed $U = 10$ m/sec duration limited case (solid line). Theoretical value of self-similar exponent $q = -3/7$ - thick horizontal dashed line.

energy dissipation areas has been observed in multiple experimental field observations and is accepted by the oceanographic community after the seminal work of Phillips (1985). One should note that most of the energy flux into the system comes in the vicinity of the spectral peak, as shown in Fig.9, providing significant inertial interval for KZ spectrum.

The angular spectral distribution of energy, presented in Fig.10, is consistent with the results of experimental observations that show a broadening of the angular spreading in both directions away from the spectral peak frequency.

To compare the duration limited numerical simulation results with the experimental analysis by Resio et al. (2004a), presented in Fig.1, Fig.11 shows the function $\beta = F(k) \cdot k^{5/2}$ as the function of $(u_\lambda^2 C_p)^{1/3}/g^{1/2}$ for wind speed $U = 10$ m/sec, along with the regression line from Resio et al. (2004a) and theoretical prediction Eq.(25) for $\lambda = 2.74$. The numerical results and theoretical prediction line fall within a very small RMS deviation ($r^2 = 0.939$, see Fig.1) from the regression line. One should note asymptotic convergence of the numerical simulation results to the theoretical line.

4.2 Limited fetch numerical simulations

The limited fetch simulation was performed in the framework of the stationary version of Eq.(1):

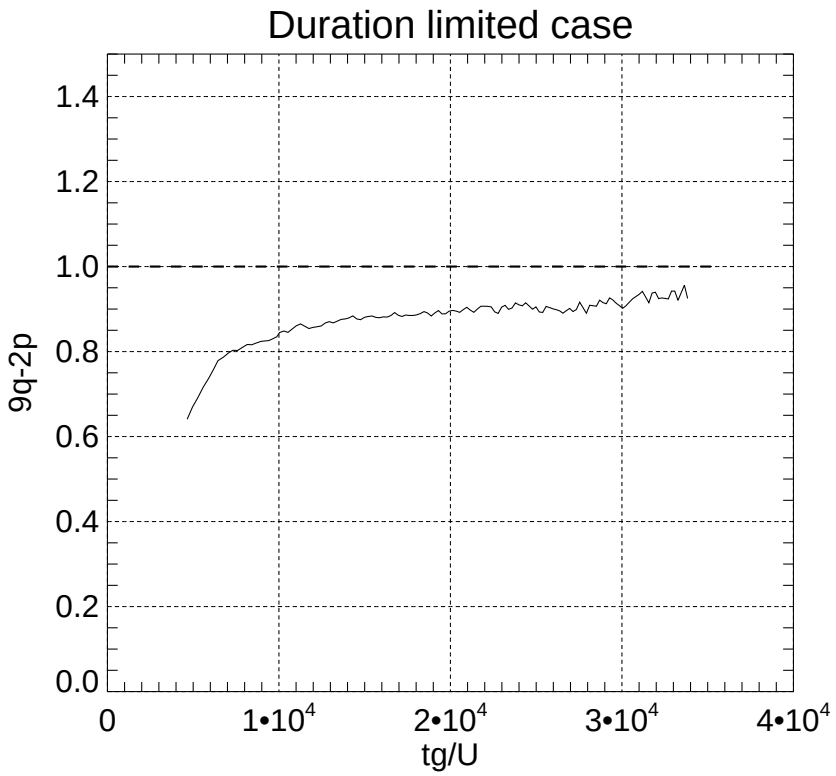

Figure 6. "Magic number" $9q - 2p$ as the function of dimensionless time tg/U for wind speed $U = 10$ m/sec duration limited case - solid line. The target value 1 for the self-similar relation Eq.(30) is presented by the horizontal dashed line.

$$\frac{1}{2}\frac{g\cos\theta}{\omega}\frac{\partial\epsilon}{\partial x} = S_{nl}(\epsilon) + S_{wind} + S_{diss} \tag{46}$$

where $\boldsymbol{x}$ is chosen as the coordinate axis orthogonal to the shore and θ is the angle between individual wavenumber $\boldsymbol{k}$ and the axis $\boldsymbol{x}$. To find the dependence on the wind speed, directed off the shore, two numerical simulations for wind speeds of $U = 5$ m/sec and $U = 10$ m/sec have been performed.

The stationarity in Eq.(46) is somewhat difficult for numerical simulation, since it contains a singularity in the form of $\cos\theta$ in front of $\frac{\partial\epsilon}{\partial x}$. This problem was overcome by zeroing one half of the Fourier space of the system for the waves propagating toward the shore. Since the energy in such waves is small with respect to waves propagating in the offshore direction, such an approximation is quite reasonable for our purposes.

Since the wind forcing index s in the fetch-limited case is similar to that in the duration limited case, the numerical simulation of Eq.(46) has been performed for the same input functions as in the duration limited case with the same low-level energy noise initial conditions in Fourier space.

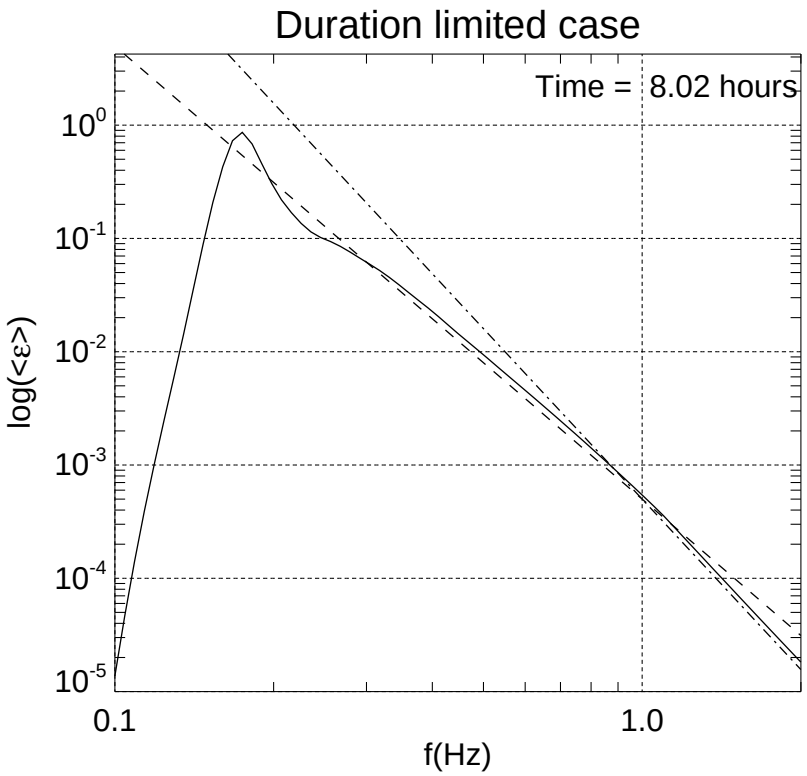

Figure 7. Decimal logarithm of the angle averaged spectrum as the function of the decimal logarithm of the frequency for wind speed $U = 10$ m/sec duration limited case - solid line. Spectrum $\sim f^{-4}$ - dashed line, spectrum $\sim f^{-5}$ - dash-dotted line.

Fig.12 presents total energy growth as a function of fetch, consistent with self-similar solution Eq.(38) for index $p = 1$, and its appropriate empirical coefficient. The corresponding values of indices p along the fetch are presented on Fig.13.

As it was noted above, the wave evolution for wind speed $U = 5$ m/sec case is expected to be slower than for $U = 10$ m/sec case due to weaker nonlinear interaction term. One can see, indeed, slower asymptotic convergence of the calculated total energy local power index to the target value $p = 1$ for $U = 5$ m/sec case, being compared to $U = 10$ m/sec case. The deviation of results from the $U = 10$ m/sec case relative to the target value does not exceed an error of about 5%, while for $U = 5$ m/sec case the error doesn't exceed 20%. The role of relatively short in time non-self-similar development of the wave system at the very beginning of the fetch should be noted as well as the factor contributing to the deviation from the target value of index p=1: the wave system obviously needs some time to get evolve into fully self-similar mode.

The small amplitude oscillations observed on Fig.13 are supposed to be attributed to the limited number of quadruplets used in the simulation.

The dependence of the mean frequency on the fetch, shown on Fig.14, is consistent with the self-similar dependence Eq.(40) for index $q = 0.3$, supplied with the empirical coefficient in front of it.

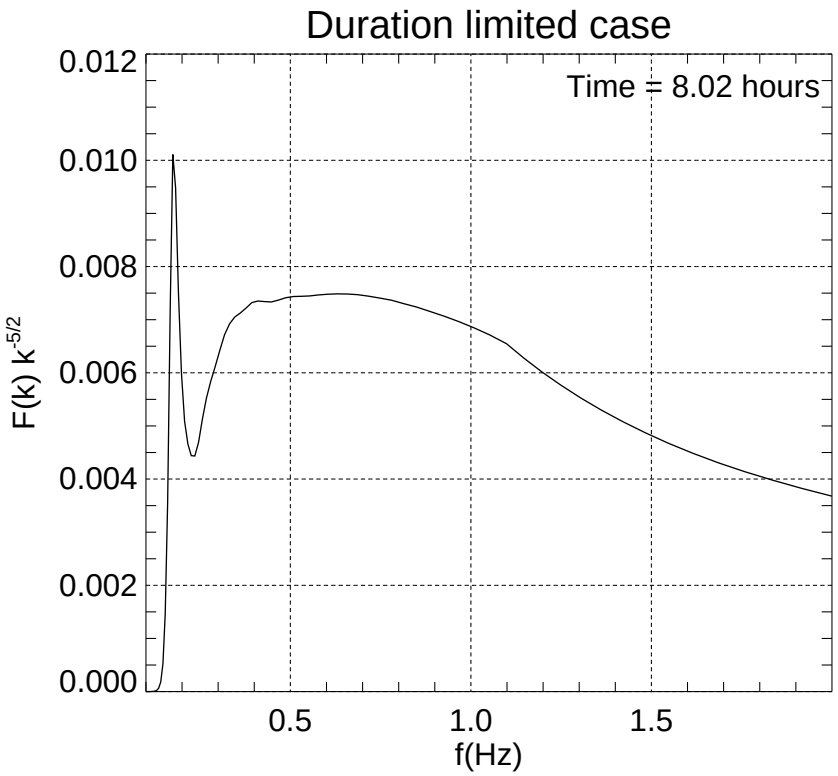

Figure 8. Compensated spectrum for duration limited case as the function of linear frequency f for wind speed $U = 10$ m/sec duration limited case.

The local values of indices q for two different wind speed amplitudes are presented on Fig.15 along with the target value of self-similar index $q = -0.3$. After suffucient fetch one can see only about 14% deviation from the target value for $U = 10$ m/sec case and about 2.5% for $U = 5$ m/sec case.

The reasons for the 10% systematic deviation from the self-similar solutions observed in the lines on Fig.14, corresponding to the wind speeds of $U = 5$ m/sec and $U = 10$ m/sec, are the same as noted previously for wave energy behavior - the transition process in the beginning of the simulation and asymptotic nature of self-similar solution.

The check on the consistency of calculated "magic number" $(10q - 2p)$ (see Eq.(36)) is presented in Fig.16. The reason of systematic deviation from the target value 1 is obviously connected the systematic deviations of p and q, as the "magic number" is calculated as their linear combination, reaching the accuracy of approximately 10% for fetches $3 \cdot 10^4$.

One should note that indices p, q and the "magic relation" $10q - 2p$ exhibit asymptotic convergence to the corresponding target values.

Fig.17 presents directionally-integrated energy spectrum, as the function of frequency, in logarithmic coordinates. As could be seen in the duration-limited case, one can see that it consists of three process-related segments:

- the spectral peak region

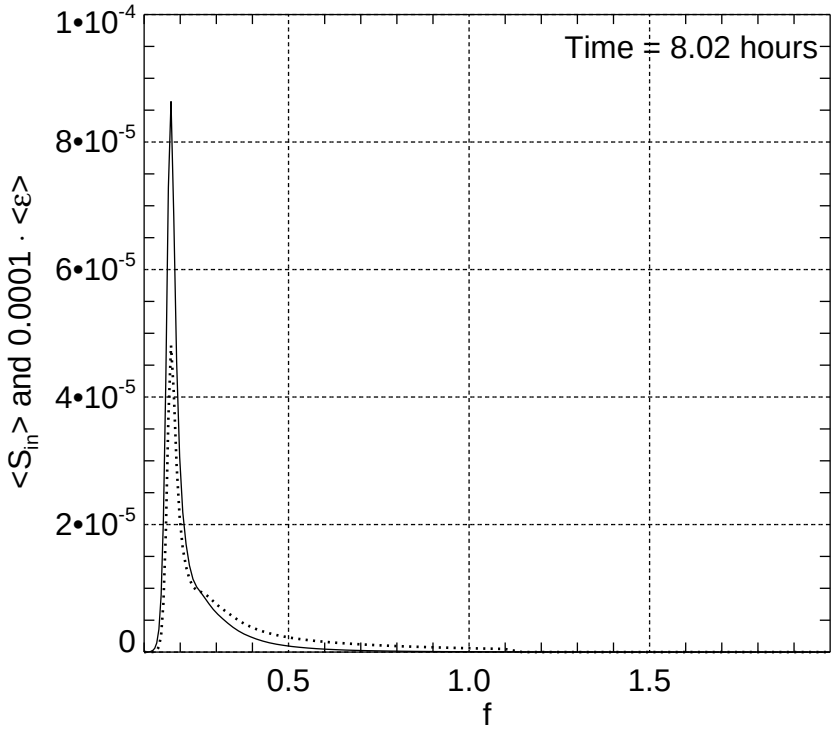

Figure 9. Typical, angle averaged, wind input function density $< S_{in} >= \frac{1}{2\pi}\int \gamma(\omega,\theta)\varepsilon(\omega,\theta)d\theta$ (dotted line) and angle averaged spectrum $< \varepsilon >= \frac{1}{2\pi}\int \varepsilon(\omega,\theta)d\theta$ (solid line) as the functions of the frequency $f = \frac{\omega}{2\pi}$ for wind speed $U = 10$ m/sec duration limited case.

- the inertial (equilibrium) range ω^{-4} spanning from the spectral peak to the beginning of the "implicit dissipation" $f = 1.1$ Hz
- Phillips high frequency tail ω^{-5} starting approximately at $f = 1.1$ Hz

The compensated spectrum $F(k)\cdot k^{5/2}$ is presented in Fig.19. One can see plateau-like region responsible for $k^{-5/2}$ behavior, equivalent to ω^{-4} tail in Fig.17. As in the duration limited case, the KZ solution (Zakharov and Filonenko, 1967) also holds for the fetch limited case, and most of the energy flux into the system comes in the vicinity of the spectral peak as well, as shown in Fig.18, providing significant inertial (equilibrium) range for KZ spectrum between spectral peak energy input and high-frequency energy dissipation areas .

The angular spectral distribution of energy, presented in Fig.20, as in the duration limited case, is consistent with the results of experimental observations that show a broadening of the angular spreading in both directions away from the spectral peak frequency.

To compare the limited fetch numerical simulation results with the experimental analysis by Resio et al. (2004a), presented in Fig.1, Fig.21 shows the function $\beta = F(k)\cdot k^{5/2}$ as a function of $(u_\lambda^2 C_p)^{1/3}/g^{1/2}$ for wind speed $U = 10.0$ m/sec, along with the regression line from Resio et al. (2004a) and its theoretical prediction Eq.(25) for $\lambda = 2.11$. The numerical results

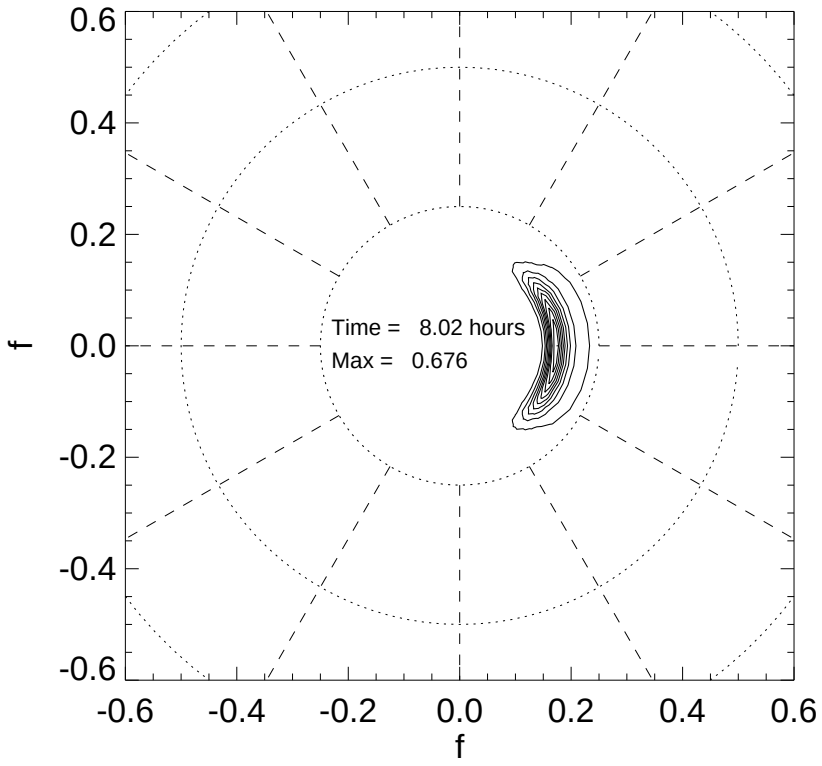

Figure 10. Angular spectra dependence for wind speed $U = 10$ m/sec duration limited case.

and theoretical prediction line fall within RMS deviation ($r^2 = 0.939$, see Fig.1) from the regression line. One should note asymptotic convergence of the numerical simulation results to the theoretical line. Being parameterized by fetch coordinate, the numerical simulation results evolve from the left to the right on the graph, from dimensionless fetch equal 0 to $3.0 \cdot 10^4$.

5 Comparison with the experiments

The comparison of limited fetch and duration limited simulations with the experimental results by Resio and Long (2007) and the theoretical prediction based on Eq.(8) is presented in Fig.11 and Fig.21. One should note that the numerical results and theoretical prediction line with corresponding values of λ fall into the RMS deviation ($r^2 = 0.939$, see Fig.1) relative to the experimental regression line Eq.(8).

The dependence of dimensionless energy and frequency on dimensionless fetch for the limited fetch simulation, superimposed on the experimental observations collected by Young (1999), are presented of Fig.22 and Fig.23. One should note consistency of the presented numerical results with these experimental observations.

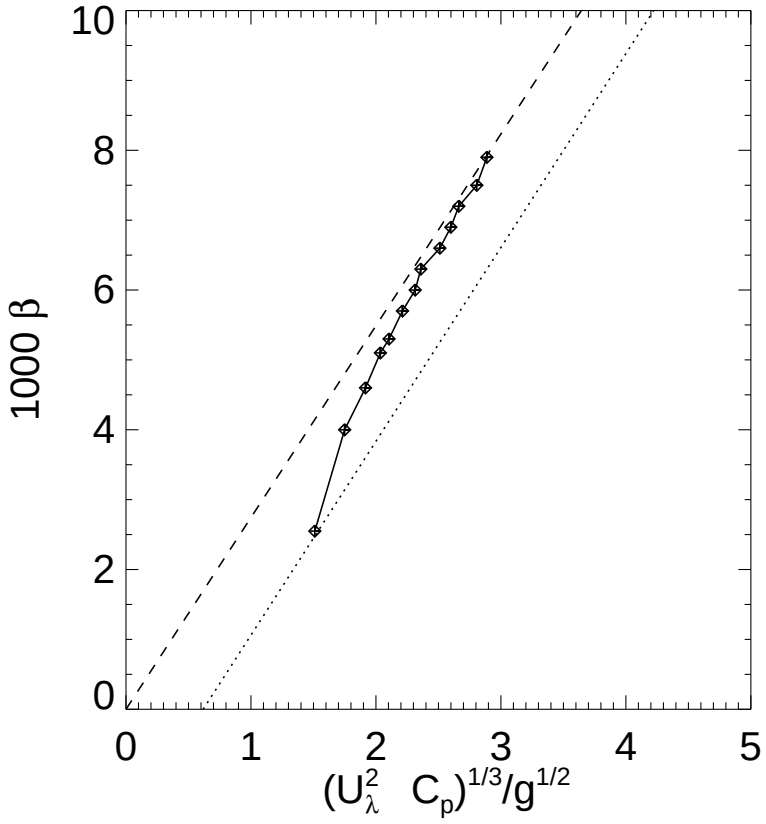

Figure 11. Experimental, theoretical and numerical evidence of the dependence of 1000β on $\left(u_\lambda^2 c_p\right)^{1/3}/g^{1/2}$. Dashed line - theoretical prediction Eq.(8) for $\lambda = 2.74$; dotted line - experimental regression line from Resio et al. (2004a); Resio and Long (2007). Line connected diamonds - results of numerical calculations for wind speed $U = 10$ m/sec duration limited case. Being parameterized by dimensionless time tg/U, the numerical simulation trajectory evolves from the left to the right on the graph, covering time span from $tg/U = 0$ to $tg/U \simeq 3.5 \cdot 10^5$.

6 Conclusions

We have analyzed the new ZRP form for wind input, proposed in Zakharov et al. (2012) in terms of both fetch-limited and duration-limited wave growth. The numerical simulations for both duration limited and fetch-imited cases, using the ZRP wind input term, XNL nonlinear term S_{nl} and "implicit" high-frequency dissipation, show remarkable consistency with predicted self-similar properties of Hasselmann equation and with the regression line from field studies relating energy levels in the equilibrium range to wind speed by Resio et al. (2004a) and Resio and Long (2007).

The authors of the research hope that this new framework will offer additional guidance for the source terms in operational models .

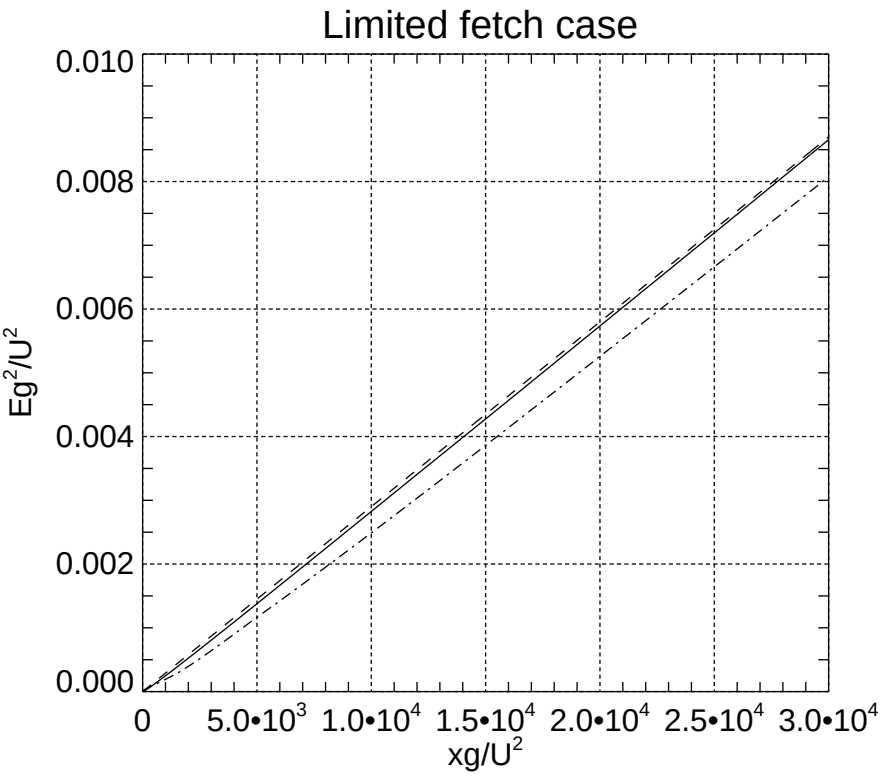

Figure 12. Dimensionless energy Eg^2/U^4 versus dimensionless fetch xg/U^2 for fetch limited case: wind speed $U = 10$ m/sec - solid line, wind speed $U = 5$ m/sec - dash-dotted line. Self-similar solution with the empirical coefficient in front of it: $2.9 \cdot 10^{-7} xg/U^2$ - dashed line.

Acknowledgements. The research presented in section 4.1 has been accomplished due to support of the grant "Wave turbulence: the theory, mathematical modeling and experiment" of the Russian Scientific Foundation No 14-22-00174. The research presented in other chapters was supported by ONR grant N00014-10-1-0991. The authors gratefully acknowledge the support of these foundations.

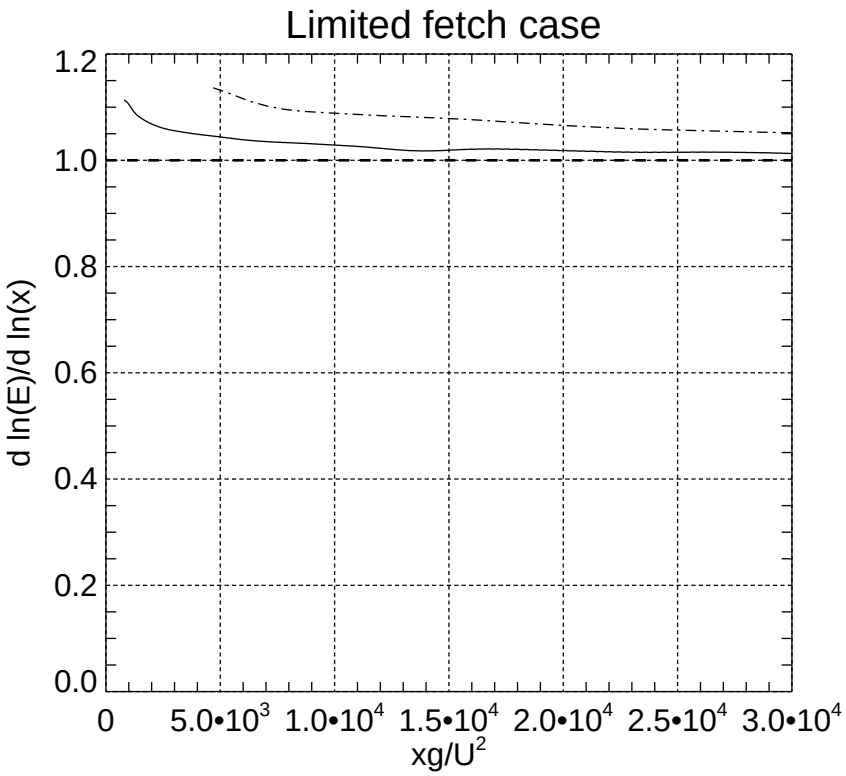

Figure 13. Energy local power function index $p = \frac{d\ln E}{d\ln x}$ as the function of dimensionless fetch xg/U^2 for fetch limited case: wind speed $U = 10$ m/sec - solid line, wind speed $U = 5$ m/sec - dash-dotted line. Theorerical value of self-similar index $p = 1$ - thick horizontal dashed line.

References

Badulin, S., Babanin, A. V., Resio, D. T., and Zakharov, V.: Weakly turbulent laws of wind-wave growth, J.Fluid Mech., 591, 339 – 378, 2007.

Badulin, S. I. and Zakharov, V. E.: The generalized Phillips' spectra and new dissipation function for wind-driven seas, arXiv:1212.0963 [physics.ao-ph], pp. 1 – 16, 2012.

Badulin, S. I., Pushkarev, A. N., D.Resio, and Zakharov, V. E.: Self-similarity of wind-driven sea, Nonlinear Proc. in Geophysics, 12, 891 – 945, 2005.

Charnock, H.: Wind stress on a water surface, Q.J.R. Meteorol. Soc., 81, 639 – 640, 1955.

Dyachenko, A. I., Kachulin, D. I., and Zakharov, V. E.: Evolution of one-dimensional wind-driven sea spectra, JETP Letters, 102, 577 – 581, 2015.

Golitsyn, G.: The Energy Cycle of Wind Waves on the Sea Surface, Izvestiya, Atmospheric and Oceanic Physics, 46, 6–13, 2010.

Hasselmann, K.: On the non-linear energy transfer in a gravity-wave spectrum. Part 1. General theory, Journal of Fluid Mechanics, 12, 481 – 500, 1962.

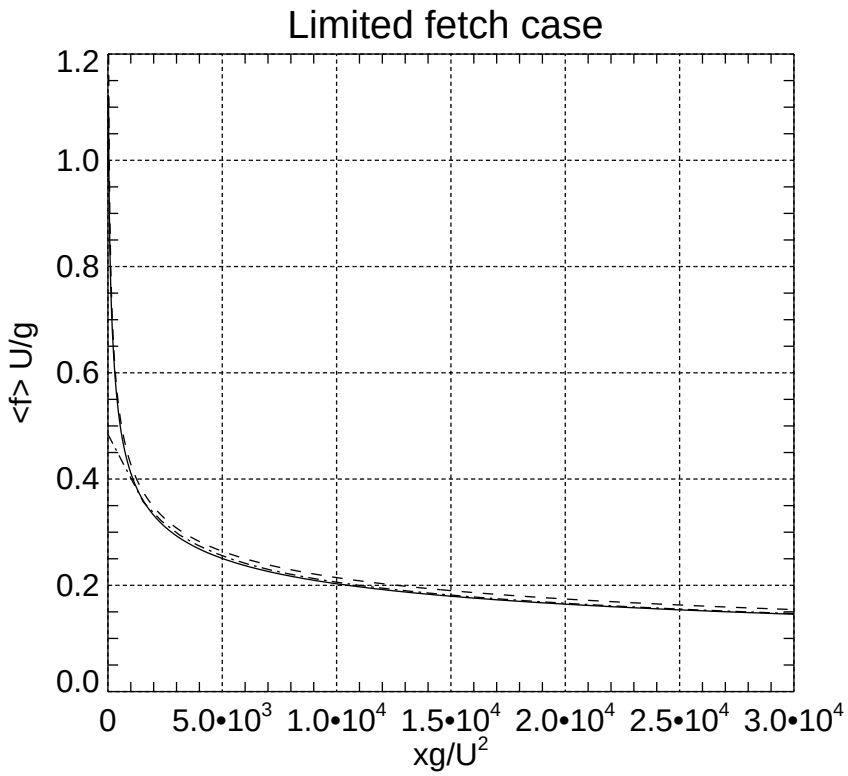

Figure 14. Dimensionless mean frequency, as the function of dimensionless fetch, calculated as $< f >= \frac{1}{2\pi} \frac{\int \omega n d\omega d\theta}{\int n d\omega d\theta}$, where $n(\omega, \theta) = \frac{\varepsilon(\omega,\theta)}{\omega}$ is the wave action spectrum, for wind speed 10 m/sec (solid line) and 5 m/sec (dashed line). The dash-dotted line is the self-similar dependence $3.4 \cdot \left(\frac{xg}{U^2}\right)^{-0.3}$ with the empirical coefficient in front of it.

Hasselmann, K.: On the non-linear energy transfer in a gravity wave spectrum. Part 2. Conservation theorems; wave-particle analogy; irrevesibility, Journal of Fluid Mechanics, 15, 273 – 281, 1963.

Irisov, V. and Voronovich, A.: Numerical Simulation of Wave Breaking, Journal of Physical Oceanography, 41, 346 – 364, 2011.

Janssen, P.: The Interaction of Ocean Waves and Wind, Cambridge monographs on mechanics and applied mathematics, Cambridge U.P., 2009.

Korotkevich, A. O., Pushkarev, A. N., Resio, D., and Zakharov, V. E.: Numerical verification of the weak turbulent model for swell evolution, Eur. J. Mech. B - Fluids, 27, 361 – 387, 2008.

Long, C. and Resio, D.: Wind wave spectral observations in Currituck Sound, North Carolina, JGR, 112, C05 001, 2007.

Longuet-Higgins, M. S.: A technique for time-dependent, free-surface flow, Proc.R.Soc.Lond. A, 371, 441 – 451, 1980a.

Longuet-Higgins, M. S.: On the forming of sharp corners at a free surface, Proc.R.Soc.Lond. A, 371, 453 – 478, 1980b.

Nordheim, L. W.: On the Kinetic Method in the New Statistics and Its Application in the Electron Theory of Conductivity, Proc. R. Soc. Lond. A, 119, 689 – 698, 1928.

Perrie, W. and Zakharov, V. E.: The equilibrium range cascades of wind-generated waves, Eur. J. Mech. B/Fluids, 18, 365 – 371, 1999.

Phillips, O. M.: The dynamics of the upper ocean, Cambridge monographs on mechanics and applied mathematics, Cambridge U.P., 1966.

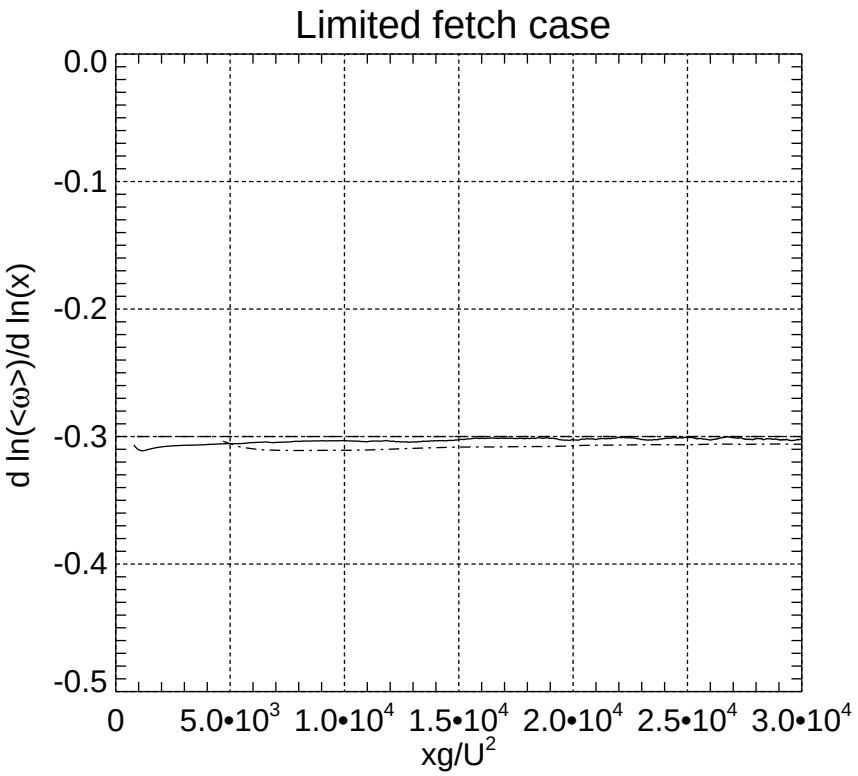

Figure 15. Local mean frequency exponent $-q = \frac{d\ln<\omega>}{d\ln x}$ as the function of dimensionless fetch xg/U^2 for fetch limited case. Wind speed $U = 10$ m/sec - solid line, wind speed $U = 5$ m/sec - dashed line. Horizontal dashed line - target value of the self-similar exponent $q = 0.3$.

Phillips, O. M.: Spectral and statistical properties of the equilibrium range in wind-generated gravity waves, Journal of Fluid Mechanics, pp. 505 – 531, 1985.

Pushkarev, A. and Zakharov, V.: Limited fetch revisited: comparison of wind input terms, in surface wave modeling, Ocean Modeling, 103, 18 — 37, doi:10.1016/j.ocemod.2016.03.005, 2016.

Resio, D. and Perrie, W.: Implications of an f^{-4} equilibrium range for wind-generated waves, JPO, 19, 193 – 204, 1989.

Resio, D. T. and Long, C. E.: Wind wave spectral observations in Currituck Sound, North Carolina, J. Geophys. Res., 112, C05 001, 2007.

Resio, D. T. and Perrie, W.: A numerical study of nonlinear energy fluxes due to wave-wave interactions in a wave spectrum. Part I: Methodology and basic results, J. Fluid Mech., 223, 603 – 629, 1991.

Resio, D. T., Long, C. E., and Vincent, C. L.: Equilibrium-range constant in wind-generated wave spectra, J. Geophys. Res., 109, C01 018, 2004a.

Resio, D. T., Long, C. E., and Vincent, C. L.: Equilibrium-range constant in wind-generated wave spectra, JGR, 109, CO1018, 2004b.

SWAN: http://swanmodel.sourceforge.net/, 2015.

Tolman, H. L.: User manual and system documentation of WAVEWATCH III, Environmental Modeling Center, Marine Modeling and Analysis Branch, 2013.

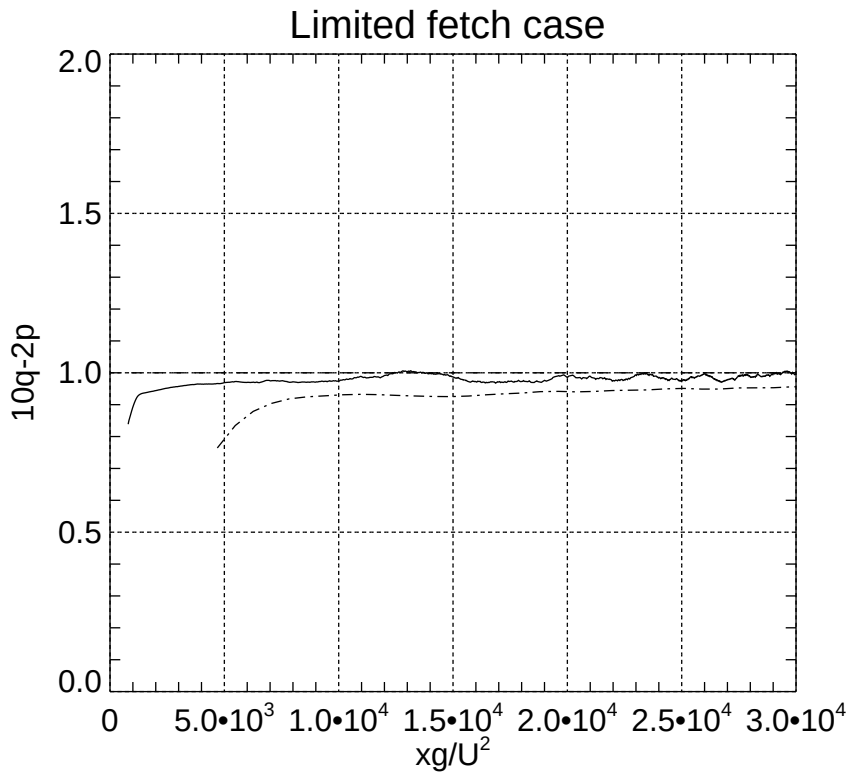

Figure 16. "Magic number" $10q - 2p$ as a function of dimensionless fetch xg/U^2 for fetch limited case. Wind speed $U = 10$ m/sec - solid line, wind speed $U = 5$ m/sec - dashed line. Horizontal dashed line - self-similar target value $10q - 2p = 1$.

Tracy, B. and Resio, D.: Theory and calculation of the nonlinear energy transfer between sea waves in deep water, WES report 11, U.S. Army Engineer Waterways Experiment Station, Vicksburg, MS, 1982.

Webb, D. J.: Non-linear transfers between sea waves, Deep-Sea Res., 25, 279 – 298, 1978.

Young, I. R.: Wind Generated Ocean Waves, Elsevier, 1999.

Zakharov, V. E.: Theoretical interpretation of fetch-limited wind-driven sea observations, NPG, 13, 1 – 16, 2005.

Zakharov, V. E.: Energy balances in a wind-driven sea, Physica Scripta, T142, 014 052, 2010.

Zakharov, V. E. and Badulin, S. I.: On energy balance in wind-driven sea, Doklady Akademii Nauk, 440, 691 – 695, 2011.

Zakharov, V. E. and Filonenko, N. N.: The energy spectrum for stochastic oscillation of a fluid's surface, Dokl.Akad.Nauk., 170, 1992 – 1995, 1966.

Zakharov, V. E. and Filonenko, N. N.: The energy spectrum for stochastic oscillations of a fluid surface, Sov. Phys. Docl., 11, 881 – 884, 1967.

Zakharov, V. E., L'vov, V. S., and Falkovich, G.: Kolmogorov Spectra of Turbulence I: Wave Turbulence, Springer-Verlag, 1992.

Zakharov, V. E., Korotkevich, A. O., and Prokofiev, A. O.: On Dissipation Function of Ocean Waves due to Whitecapping, in: American Institute of Physics Conference Series, edited by Simos, T. E., G.Psihoyios, and Tsitouras, C., vol. 1168, pp. 1229 – 1237, 2009.

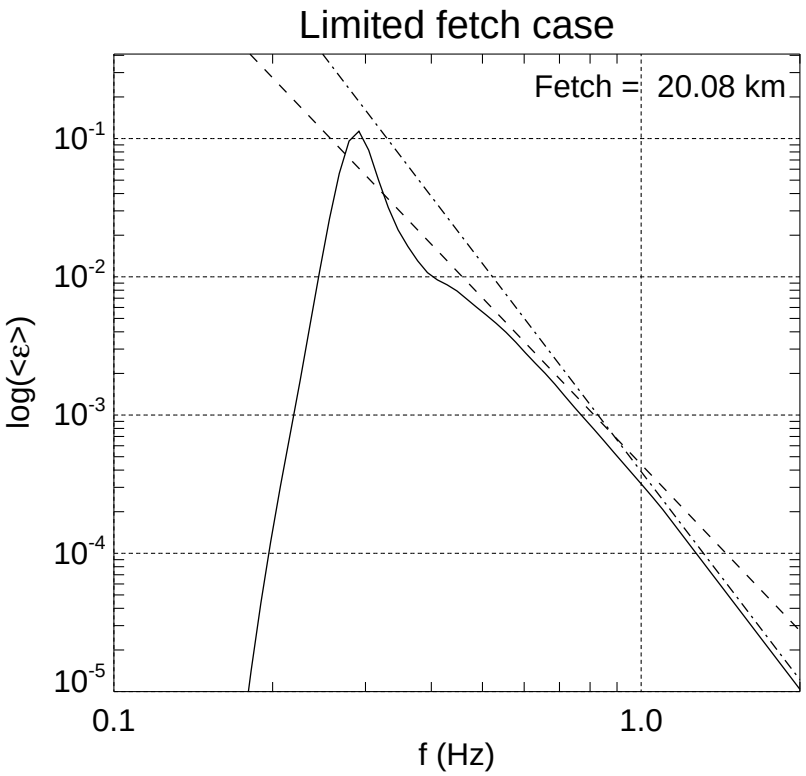

Figure 17. Decimal logarithm of the angle averaged spectrum as the function of the decimal logarithm of the frequency for wind speed $U = 10$ m/sec duration limited case- solid line. Spectrum $\sim f^{-4}$ - dashed line, spectrum $\sim f^{-5}$ - dash-dotted line.

Zakharov, V. E., Resio, D., and Pushkarev, A.: New wind input term consistent with experimental, theoretical and numerical considerations, http://arxiv.org/abs/1212.1069/, 2012.

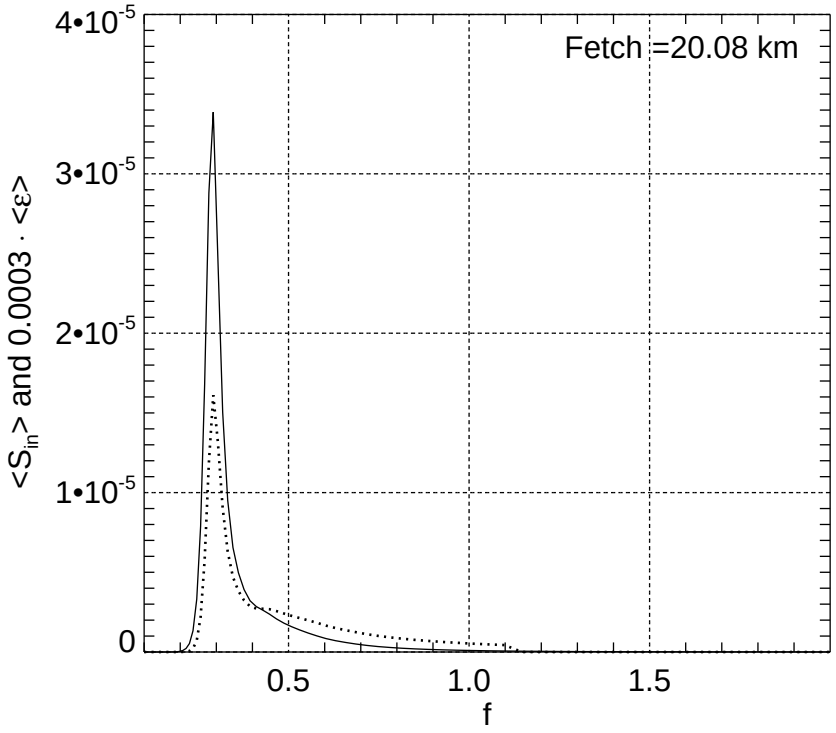

Figure 18. Typical, angle averaged, wind input function density $< S_{in} >= \frac{1}{2\pi}\int \gamma(\omega,\theta)\varepsilon(\omega,\theta)d\theta$ (dotted line) and angle averaged spectrum $< \varepsilon >= \frac{1}{2\pi}\int \varepsilon(\omega,\theta)d\theta$ (solid line) as the functions of the frequency $f = \frac{\omega}{2\pi}$ for $U = 10$ m/sec fetch limited case.

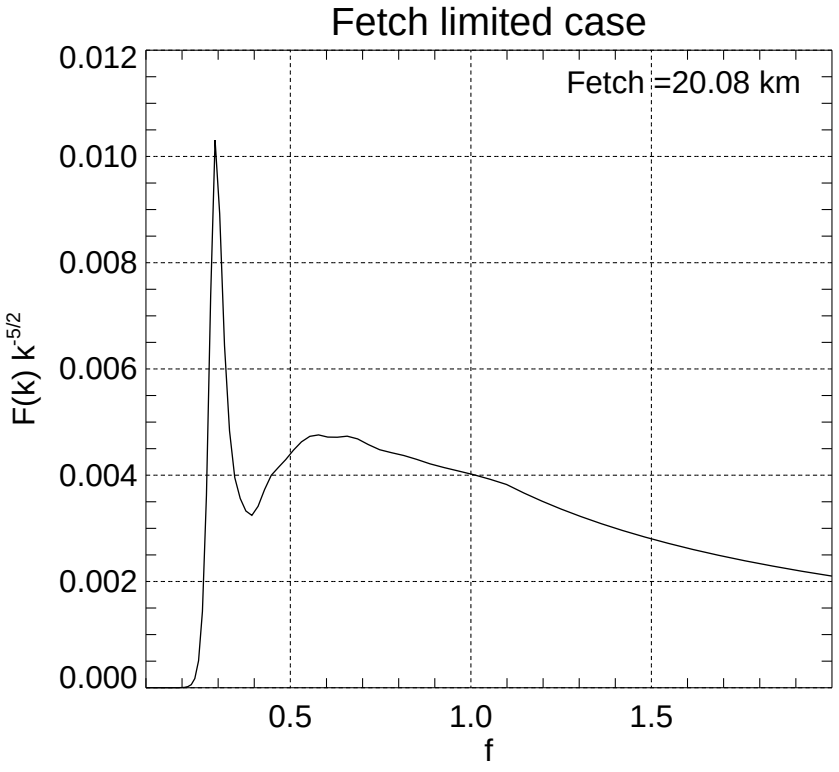

Figure 19. Compensated spectrum for fetch limited case as the function of linear frequency f for wind speed 10 m/sec fetch limited case.

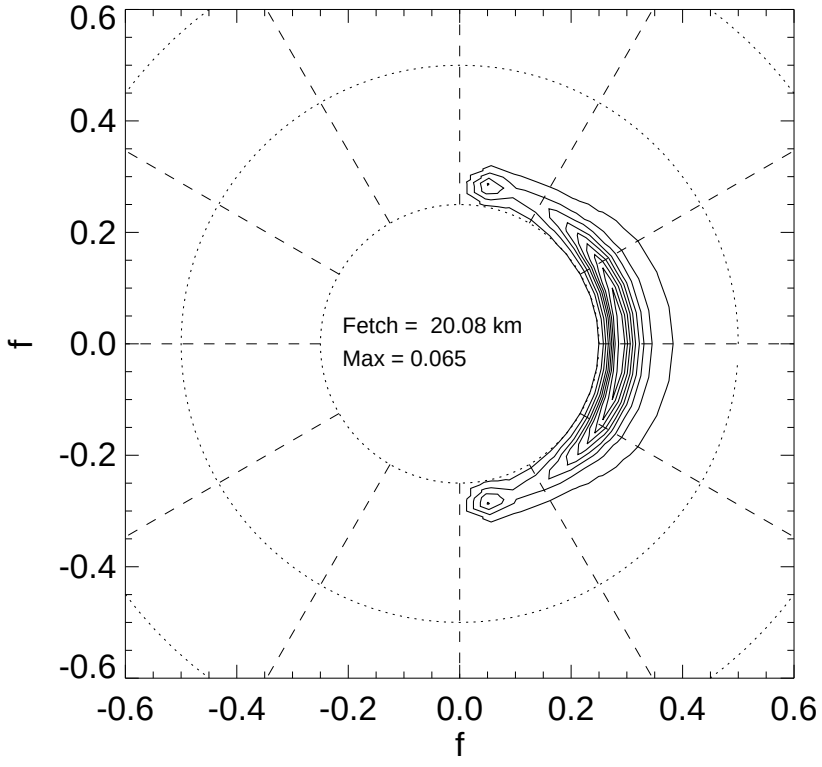

Figure 20. Angular spectra for wind speed $U = 10$ m/sec fetch limited case.

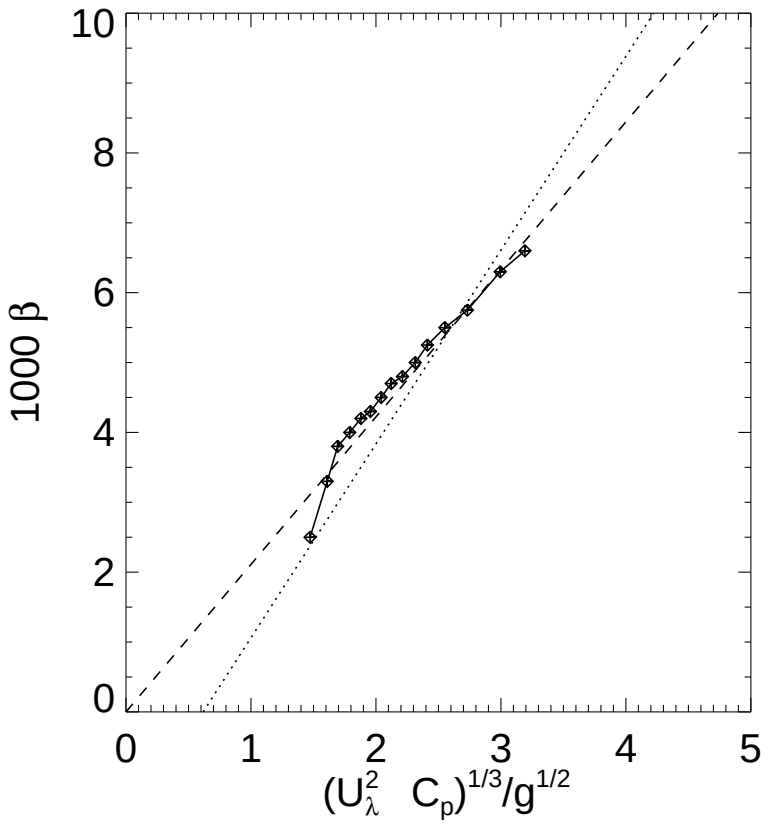

Figure 21. Experimental, theoretical and numerical evidence of the dependence of 1000β on $\left(u_\lambda^2 c_p\right)^{1/3}/g^{1/2}$. Dashed line - theoretical prediction Eq.(8) for $\lambda = 2.11$; dotted line - experimental regression line from Resio et al. (2004a); Resio and Long (2007). Line connected diamonds - the results of numerical calculations for wind speed $U = 10$ m/sec fetch limited case. Being parameterized by dimensionless fetch coordinate $\chi = \frac{xg}{U^2}$, the numerical simulation trajectory evolves from the left to the right on the graph, covering fetch span from $\chi = 0.$ to $\chi \simeq 3.0 \cdot 10^4$.

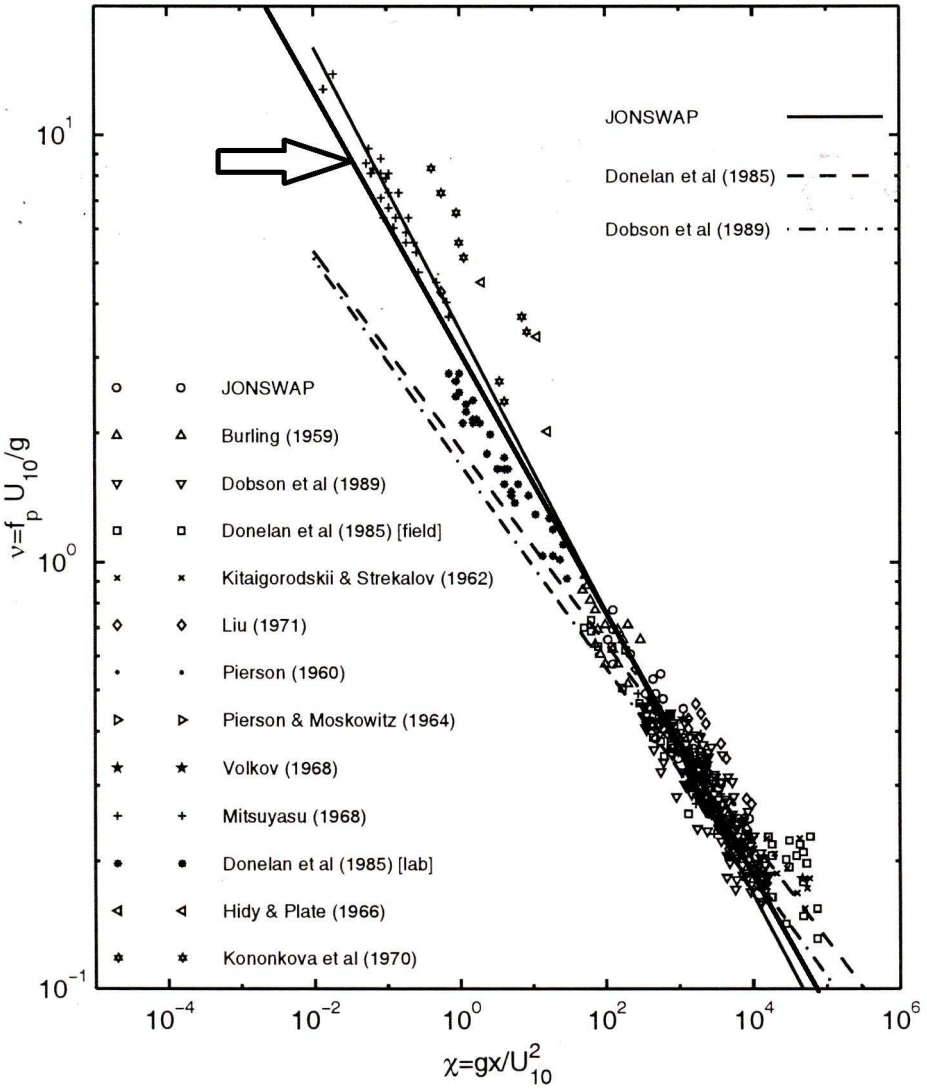

Figure 22. Solid line (pointed by arrow), presents nondimentional energy ε from the limited fetch numerical experiments, superimposed on the Figure 5.4, which is adapted from Young (1999). The original caption is: "A composite of data from variety of studies showing the development of the non-dimensional energy, ε as a function of non-dimensional fetch, χ. The original JONSWAP study (Hasselmann et al, 1973) used the data marked, JONSWAP, together with that of Burling (1959) and Mitsuyasu (1968). Also shown are a number of growth curves obtained from the various data sets. These include: JONSWAP Eq.(5.27), Donelan et al (1985) Eq,(5.33) and Dobson et al (1989) Eq.(5.38)."

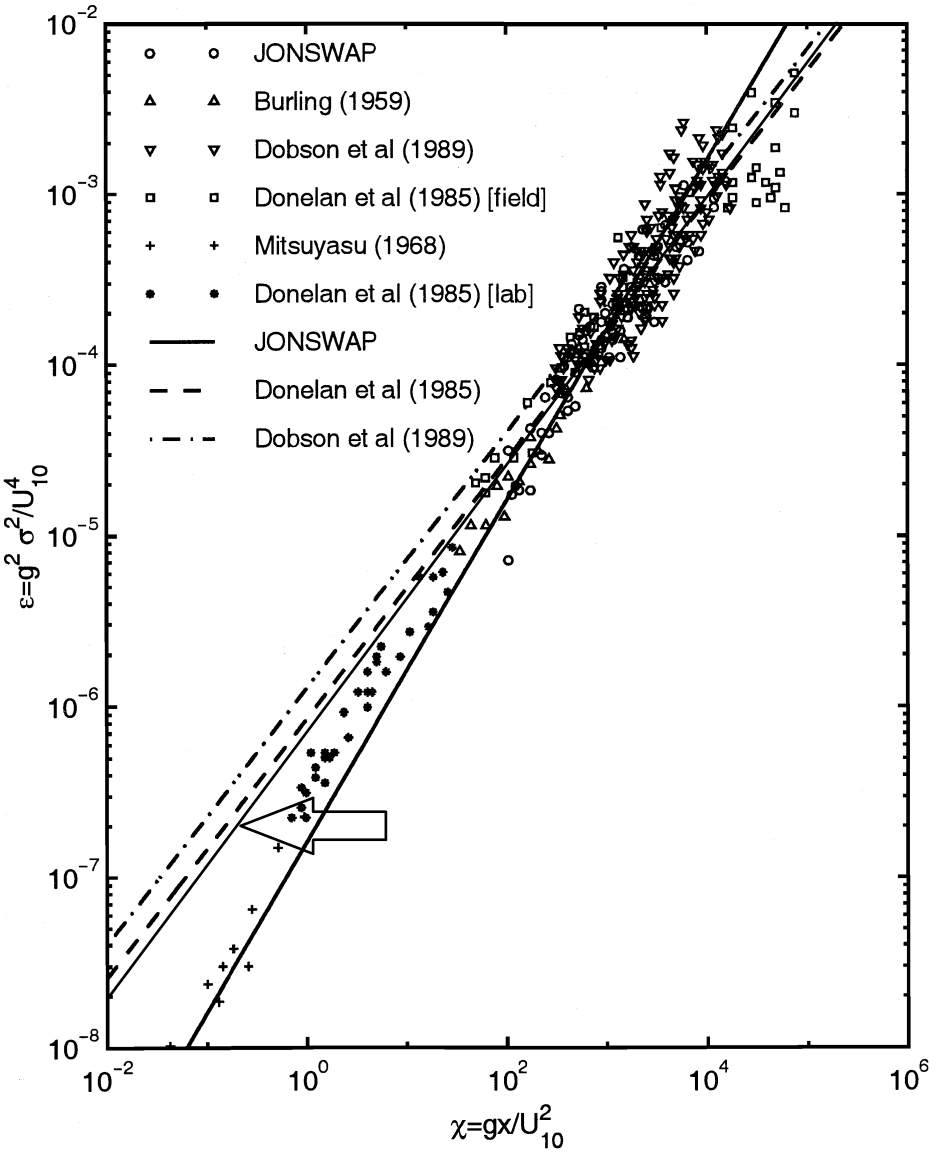

Figure 23. Solid line (pointed by arrow), presents non-dimensional frequency as the function of the fetch for limited fetch numerical experiments, superimposed on the Figure 5.5, adapted from Young (1999). The original caption is: "A composite of data from a variety of studies showing the development of the non-dimensional peak frequency, ν as a function of non-dimensional fetch, χ. The original JONSWAP study (Hasselmann et al, 1973) used all the data shown with the exception of that marked Donelan et al (1985) and Dobson et al (1989). Also shown are a number of growth curves obtained from the various data sets. These include: JONSWAP Eq.(5.28), Donelan et al (1985) Eq.(5.34) and Dobson et al (1989) Eq.(5.39)."